

EPiC Series in Computing

Volume 114, 2026, Pages 91–100

Proceedings of the Workshop on Mathematical Modeling and Scientific Computing



Neural Network Reconstruction of Control Parameters in Directed Percolation

Danil Parkhomenko[1,3], Pavel Ovchinnikov[1,2,3], Konstantin Soldatov[1,2,3], Gennady Chitov[3], and Vitalii Kapitan[4]

[1] Institute of High Technologies and Advanced Materials, Far Eastern Federal University,, Vladivostok, Russia
parkhomenko.dale@dvfu.ru
[2] Institute of Applied Mathematics, Far Eastern Branch, Russian Academy of Science, Vladivostok, Russia
[3] Bogoliubov Laboratory of Theoretical Physics, Joint Institute for Nuclear Research, Dubna, Russia
[4] Institute for Functional Intelligent Materials, National University of Singapore, Singapore
kapitanv@nus.edu.sg

Abstract

We present an extended multi-task deep learning framework for the automated identification of non-equilibrium phase transitions and physical parameter estimation in a $(1+1)$-dimensional kinetic replication probabilistic cellular automaton. Building upon a length-agnostic temporal convolutional network with a gated recurrent unit (TCN-GRU), our model now performs regression on the underlying control probabilities (p, q) directly from raw spatiotemporal configurations, in addition to classifying percolation and several renormalized states. This multi-task approach provides an efficient, data-driven methodology for phase-space localization and connectivity-based pattern recognition without handcrafted order parameters.

Keywords: Directed percolation, phase transitions, deep learning, temporal convolutional networks, gated recurrent unit.

1 Introduction

Non-equilibrium kinetics and phase transitions have been studied extensively over the past several decades. Their applications range from statistical physics to biology, ecology, and network theory [2, 6, 9, 18, 31, 34].

The central problem of these studies is the transition between active (percolating) and inactive (absorbing) phases. Unlike transitions characterized by local thermodynamic order parameters, percolation is a phase transition that probes the global connectivity of a system. It defines a specific threshold at which long-range connections form a continuous path through at least one spatial or spatiotemporal dimension. The percolating phase is characterized by the presence of a spanning cluster, and the appropriate order parameter is the fraction of sites belonging to this cluster in the thermodynamic limit. Directed percolation (DP) is the

principal universality class for such transitions. In $(1+1)$-dimensional space-time lattices, DP models a stochastic process where connectivity is restricted to a specific orientation, usually the temporal direction. DP has a wide range of applications, such as wildfire spread models [7, 17], cardiac tissue dynamics [23], and the laminar-to-turbulent transition in shear flows [10]. Broader variants, such as semi-directed percolation models, further demonstrate the robustness of DP scaling beyond standard lattice structures [11].

Cellular automata provide a classical framework for studying how local update rules generate collective behaviour and complex spatiotemporal patterns. For example, Stephen Wolfram investigated elementary cellular automata, in which binary states on a one-dimensional lattice evolve synchronously according to deterministic rules involving each site and its two nearest neighbours [35]. The kinetic replication model considered in present study uses the same neighbourhood structure, but replaces the deterministic local map with transition probabilities governed by parameters p and q. It therefore belongs to the class of probabilistic cellular automata. Statistical inference of cellular-automaton rules has also been investigated using likelihood-based methods [3]. This perspective connects our simultaneous recognition of percolation patterns and estimation of (p, q) to the broader problem of inferring local dynamics from spatiotemporal observations.

Recent studies have revealed a hidden hierarchical structure within the percolating phase. It has been shown [19,20,32,33] that the active phases of several $(1+1)$ kinetic processes possess hidden orders characterized by distinct percolative patterns, emerging at specific points of DP phase transitions. Furthermore, the active phase can exhibit a hierarchical structure known as a "tower of percolation patterns." Within this tower, increasingly complex structural orders emerge through a series of continuous transitions as the control parameters are varied [19]. From the viewpoint of percolation theory, the transition into such a phase belongs to the DP universality class [8, 18, 30].

Machine learning (ML) methods have been applied to study ground states and phase transitions in statistical physics [13, 16], including spin glasses [5, 12, 15], super-resolution of spin configurations using flow-based generative models [29], phase transitions in Heisenberg magnets [4], and thermodynamic behavior of complex spin systems [1,14,22]. Various ML algorithms have been applied to DP models: Siamese Neural Networks predict critical values and exponents by comparing configuration pairs [26]; supervised learning with Convolutional and Fully Connected Networks classifies DP phases [24]; unsupervised learning through autoencoders and principal component analysis represents the capacity of connected clusters, which is the percolation order parameter [27]; transfer learning methods identify DP critical points with limited labeled data [28]; and diffusion models have been applied to probe latent hierarchical structure in data [25].

The physical phase diagram and hierarchy of percolation patterns in the kinetic replication model were established in Refs. [19, 20]. In particular, Ref. [19] investigated finite-size and finite-time scaling of the relevant order parameters, determined critical points and exponents, and confirmed the DP universality class of the studied continuous transitions. The TCN-GRU architecture for their classification was introduced in Ref. [21]. In the present work, we extend this framework by introducing a regression head for simultaneous inference of the control parameters (p, q) and analyze the resulting prediction-error structure across the phase diagram.

2 Problem formulation

2.1 Replication model and percolation background

We study the replication process, in which the spreading of active sites follows stochastic update rules governed by two probability parameters, $p, q \in [0, 1]$. For a site to remain active at any discrete time step $t + 1$, it must be supported by at least one active precursor from the immediately preceding step t. A spanning cluster is defined as a connected set of active sites extending from the initial configuration at $t = 0$ through to the final time step. The formation of this cluster is determined by the critical values of p and q, which define the phase boundaries between the absorbing and active phases. These boundaries are well established for specific cases; for instance, when $p = 0$, the model reduces to bond directed percolation (BDP) with a known critical threshold at $q \approx 0.6447$ [8].

Within this model, Monte Carlo simulations have identified several transitions within the active phase, from simple percolation (P) to renormalized (coarse-grained) states: dipole patterns (D), quadrupole patterns (Q), and finally plaquette patterns (PL), all belonging to the DP universality class.

The state of the system at discrete time step $t = 0, 1, \ldots, T$ is specified by the occupation numbers $n_{i,t} = 0, 1$ (empty/filled), $i = 1, \ldots, N$, with periodic boundary conditions (PBC) in the spatial direction, see Fig. 1. At $t = 0$, an initial random configuration of n elements is established. The probabilistic rules presented in Table 1 and visualized in Fig. 1 are used to numerically mimic stochastic temporal evolution of the model.

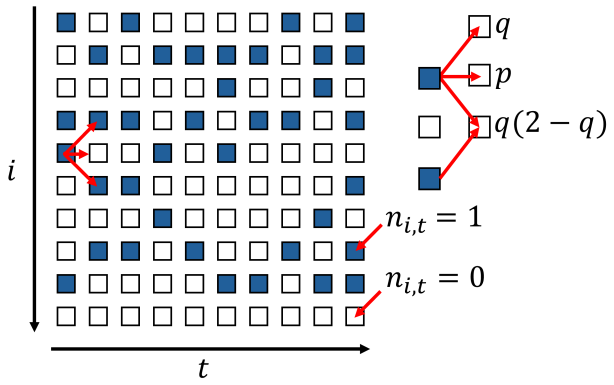

Figure 1: Space–time lattice of binary states with axes i (vertical) and t (horizontal); filled blue cells denote $n_{i,t} = 1$, empty cells $n_{i,t} = 0$. Local stochastic update rules: survival of the center with probability p, activation from each neighbor with probability q; two active neighbors yield $q(2 - q)$.

2.2 Percolation patterns

The notion of the percolative backbone (we will call it "pattern" in the present study) was defined in [33] as percolation on the backbone cluster spanning through the whole system. This cluster consists of renormalized (coarse-grained) nodes made out of a chosen subset of nodes

Table 1: Stochastic update rules.

$(n_{i-1,t}, n_{i,t}, n_{i+1,t})$	Probability of $n_{i,t+1} = 1$
$(1,1,1), (1,1,0), (0,1,1), (0,1,0)$	p
$(0,0,1), (1,0,0)$	q
$(1,0,1)$	$q(2-q)$
$(0,0,0)$	0

of the original lattice (graph) with a particular choice of filling. The percolation occurs with respect to the bonds connecting active nodes of the backbone cluster.

Spanning is determined by an explicit graph-connectivity test. For the percolation state P, the nodes of the graph are the active nodes of the original spatiotemporal lattice, and the directed edges follow the admissible temporal connections of the stochastic update rules. For hidden patterns, the same test is applied after replacing the original nodes with the corresponding renormalized nodes, along with a specified nearest-neighbor (nn) or next-nearest-neighbor (nnn) connectivity rule. A pattern label is assigned when there exists a connected directed path of active original or renormalized nodes spanning the system in the time direction.

The percolation patterns of the replication model are illustrated in Fig. 2: simple percolation P on the original lattice and hidden renormalized (coarse-grained) states.

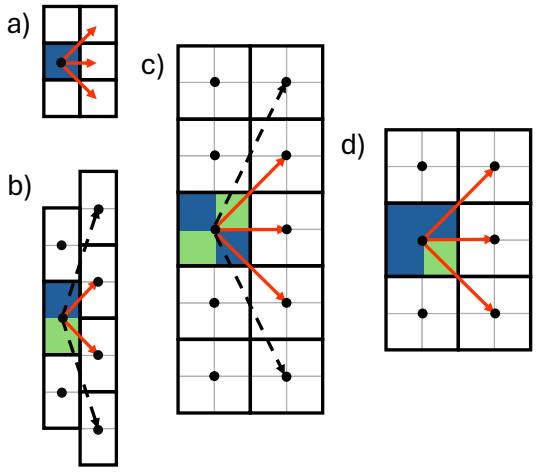

Figure 2: Schematic percolation patterns of the replication model. Active (occupied) sites are shown in blue, empty sites in green. (a) Percolation on the original lattice sites with nearest neighbors (solid red lines). (b) Dipolar percolation: phase D with nn, while phase D^+ includes also next-nearest neighbors (dashed black lines). (c) Similarly for quadrupole patterns Q and Q^+. (d) Plaquette pattern PL includes either nearest fully occupied 2×2 blocks or blocks with one empty site. The black dots mark the centers of new (coarse-grained) nodes.

Dipole patterns D (nn) and D^+ (nnn) are set as shown in Fig. 2(b). The occupation numbers on the sites of the coarse-grained (dipole) lattice for the four possible dipole configurations are

defined as follows:

$$\begin{aligned}\tilde{n}_{i,t} &= \begin{pmatrix} 1 \\ 0 \end{pmatrix} = 1, \quad \tilde{n}_{i,t} = \begin{pmatrix} 0 \\ 1 \end{pmatrix} = -1, \\ \tilde{n}_{i,t} &= \begin{pmatrix} 0 \\ 0 \end{pmatrix} = \begin{pmatrix} 1 \\ 1 \end{pmatrix} = 0.\end{aligned}$$

The site on the coarse-grained lattice is active if a dipole resides on it, $\tilde{n}_{i,t} = \pm 1$.

Quadrupole patterns Q (nn) and Q^+ (nnn) are set as shown in Fig. 2(c). The quadrupole occupation numbers on the nodes of the plaquette lattice are defined as

$$\begin{aligned}\tilde{n}_{i,t} &= \begin{pmatrix} 1 & 0 \\ 0 & 1 \end{pmatrix} = 1, \quad \tilde{n}_{i,t} = \begin{pmatrix} 0 & 1 \\ 1 & 0 \end{pmatrix} = -1, \\ \tilde{n}_{i,t} &= 0, \quad \text{for all other configurations.}\end{aligned}$$

The site is called active if $\tilde{n}_{i,t} = \pm 1$.

Plaquette patterns PL (nn) are set as shown in Fig. 2(d). There are two types of 2×2 plaquettes: fully filled or those with only one empty corner.

A detailed discussion of patterns construction is given in Ref. [19]. Assigning "active" or "inactive" labels to renormalized nodes is not unique. For any given block geometry, multiple distinct labeling schemes may be used, each producing a different percolation pattern while remaining consistent with the same underlying dynamics. For instance, for 2×2 plaquettes, one may define the quadrupole configuration as the active renormalized site and treat all other local configurations as inactive; alternatively, one may label as active only fully occupied plaquettes, or those with exactly three occupied sites.

3 Numerical algorithm

3.1 Baseline Model Architecture and Data Generation

The baseline system generates $(1+1)$-dimensional spatiotemporal configurations of a probabilistic cellular automaton (PCA) governed by stochastic update rules with parameters p, q [20]. Each configuration is stored as a Boolean array $X \in \{0,1\}^{N \times T}$ with N spatial sites and T time steps.

To detect global connectivity without handcrafted physical observables, a multi-head temporal neural network was previously developed [21]. Its architecture and classification performance are described in detail in Ref. [21]; here we retain the same TCN-GRU backbone and classification heads and add a regression head. In the original formulation, the multi-hot target vector contains the patterns of the "tower" of directed percolation patterns:

$$\{A, PL, Q^+, D^+, Q, D\}, \tag{1}$$

where A is the absorbing phase, PL the plaquette pattern, Q/Q^+ the quadrupole patterns, and D/D^+ the dipole patterns; the superscript $+$ marks patterns that also admit next-nearest-neighbour connections. The percolating head P is omitted because it is equivalent to $1 - A$. The order of the components is only a fixed convention for the output heads. The hierarchy is given by the nesting of the pattern regions on the phase diagram, $D \subset Q \subset D^+ \subset Q^+ \subset P$ and $PL \subset P$ [19, 20], so a configuration in a finer phase also carries the labels of the coarser ones.

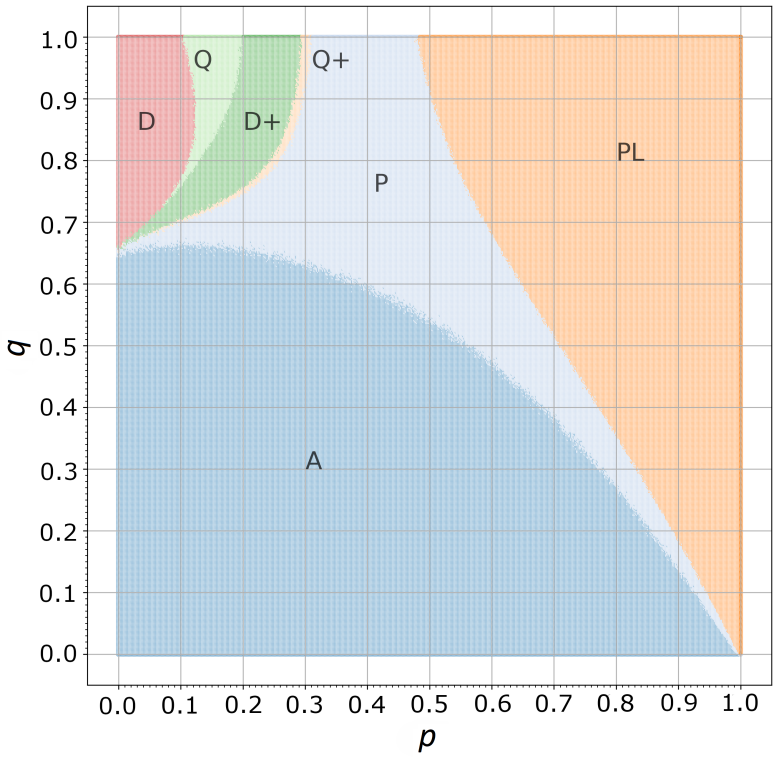

Figure 3: Simulated phase diagram for N=50, T=2000 across the (p, q) plane (see [21]). Pattern regions are color-coded: A (blue), P (light blue), PL (orange), Q^+ (light orange), D^+ (green), Q (light green), D (red).

3.2 Multi-Task Target Reconstruction (Classification & Regression)

In this work, we reassembled the dataset with an upgraded target structure to expand the model's capabilities into a multi-task learning framework.

Rather than training the neural network solely on classification, we formulate a joint classification-regression task in which the model is trained to simultaneously predict:

- The binary classification targets representing the percolation patterns $\{A, PL, Q^+, D^+, Q, D\}$
- The physical probabilities (p, q) under which each respective configuration was simulated.

This formulation encourages the shared TCN-GRU backbone to learn a shared representation that captures both the discrete topological phases and the continuous parameters of the physical system.

To rigorously test the regression performance on unseen parameter combinations and avoid overfitting, we evaluate the regression head on a dedicated Out-of-Sample (OoS) stress-test dataset. The quality of parameter estimation is measured using the Spearman Rank Correlation

Coefficient (SCC), which assesses how monotonically the predicted parameters correlate with the ground-truth physical probabilities across the phase transitions [20].

The classification heads are optimized using standard Binary Cross-Entropy loss (BCELoss). The regression head, predicting the continuous (p, q) coordinates, is trained using Mean Squared Error loss (MSELoss):

$$\mathcal{L}_{\text{MSE}} = \frac{1}{B} \sum_{i=1}^{B} \left((p_i - \hat{p}_i)^2 + (q_i - \hat{q}_i)^2 \right)$$

4 Results and discussion

The addition of the parameter-regression task enables the shared representation to encode information about the location of each configuration in the control-parameter space. On the OoS evaluation dataset, the regression head demonstrated robust generalization, achieving SCC of approximately 0.70–0.84 (Table 2). Consequently, given an arbitrary space-time configuration $X \in \{0, 1\}^{N \times T}$, the model simultaneously classifies the structural percolation pattern and infers the underlying physical control parameters (p, q) governing the kinetic replication dynamics.

Table 2: Comparison of MSE and SCC for different values of T and parameters p, q

T	500		1000		2000		3000	
	p	q	p	q	p	q	p	q
MSE	0.0329	0.0325	0.0316	0.0303	0.0313	0.0287	0.0314	0.0278
SCC	83.4%	76.4%	83.6%	74.2%	70.5%	80.1%	69.6%	80.7%

To examine the geometric fidelity of the predicted parameter manifold, we analyze the topography of parameter errors across the $(p_{\text{true}}, q_{\text{true}})$ plane and compare it with the underlying phase diagram shown in Fig. 3. For scoring, the parameters p and q were sampled uniformly at random, yielding 300,000 random parameter pairs (i.e., distinct systems), which were then processed individually. We evaluate individual predictions $\hat{p}$ and $\hat{q}$, along with the total error magnitude defined as:

$$E_{\text{mag}} = \sqrt{(\hat{p} - p_{\text{true}})^2 + (\hat{q} - q_{\text{true}})^2}$$

Furthermore, we map the model's error topology by constructing the two-dimensional vector field of prediction errors (see Fig. 4):

$$\mathbf{e}(\hat{p}, \hat{q}) = (\hat{p} - p_{\text{true}},\ \hat{q} - q_{\text{true}})$$

The resulting error field exhibits a clear and interpretable structure: in the vicinity of phase boundaries, the error vectors systematically "flow away" from critical transition lines toward the interior of stable phases. The magnitude of the regression error is highly non-uniform across the control parameter plane, whereas the vector field exhibits an ordered orientation near the primary phase transition boundaries.

On a macroscopic scale, the spatial organization of the error field naturally outlines the primary topology of the underlying phase diagram. Because the regression head is optimized strictly on the continuous control parameters (p, q), without explicit conditioning on internal coarse-grained order parameters, the network primarily resolves the main macroscopic boundaries A, P, PL while smoothing the fine-grained hidden sub-pattern transitions D, D^+, Q, Q^+.

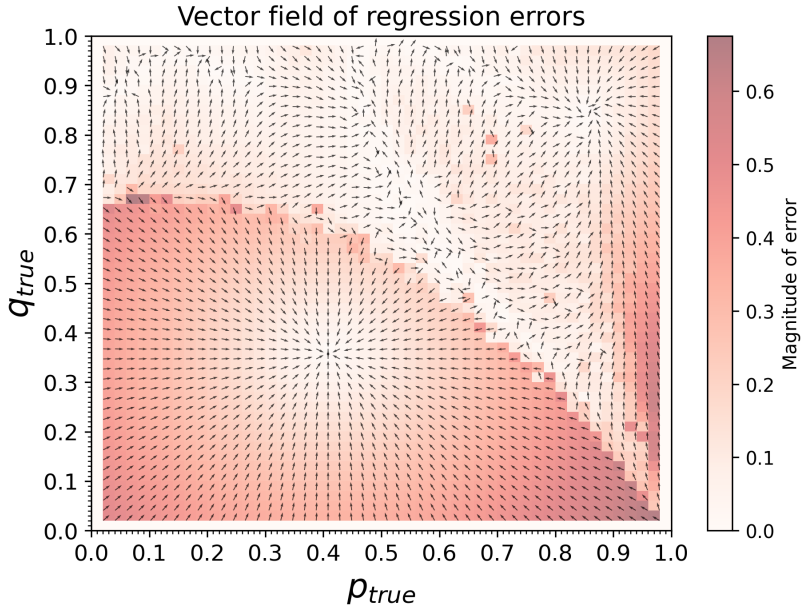

Figure 4: Prediction error topology and magnitude across the phase space $(p_{\text{true}}, q_{\text{true}})$. The underlying heatmap displays the total prediction error magnitude E_{mag}. The overlaid vector field depicts the direction and extent of parameter deviations $\mathbf{e}(\hat{p}, \hat{q})$.

5 Conclusion

In this work, we presented an extended multi-task deep learning framework that unifies topological pattern classification and physical parameter regression for $(1+1)$-dimensional kinetic replication processes. By upgrading the baseline TCN-GRU architecture, the model simultaneously identifies the hierarchical "tower" of directed percolation patterns $\{A, PL, Q^+, D^+, Q, D\}$ and predicts the continuous control probabilities (p, q) directly from raw spatiotemporal configurations.

Our evaluation on OoS configurations shows that the regression head, trained jointly with the classification heads on a shared TCN–GRU backbone, recovers the control parameters p and q with SCC of 70%–85% and a mean squared error of about 0.03, demonstrating strong generalization. Furthermore, topological analysis of the prediction error vector field $\mathbf{e}(p, q)$ revealed that parameter errors naturally flow away from continuous phase transition boundaries toward the stable interiors of primary phases, such as the absorbing (A) and plaquette (PL) states. This behavior indicates that the shared latent representations preserve both the discrete connectivity transitions and the continuous parameter manifold without relying on handcrafted order parameters.

The proposed approach offers a computationally efficient, length-agnostic tool for rapid phase mapping and parameter estimation in probabilistic cellular automata and related non-equilibrium systems. Future research will focus on extending this multi-task methodology to higher-dimensional lattices, complex empirical networks, and real-time detection of critical phenomena in experimental non-equilibrium dynamics.

Acknowledgements

This research was financially supported by a grant # 25-21-00286, https://rscf.ru/project/25-21-00286/ from the Russian Science Foundation.

References

[1] P. Andriushchenko, D. Kapitan, and V. Kapitan. A new look at the spin glass problem from a deep learning perspective. *Entropy*, 24(5):697, 2022.

[2] A.-L. Barabási. *Network Science*. Cambridge University Press, Cambridge, UK, 2016.

[3] R.V. Craiu and T.C.M. Lee. Pattern generation using likelihood inference for cellular automata. *IEEE transactions on image processing*, 15(7):1718–1727, 2006.

[4] D.A. Druz'ev, A.A. Chubarova, and P.V. Prudnikov. Phase transitions in Heisenberg magnets induced by uniaxial anisotropy: Wang–Landau and machine learning simulations. *JETP Letters*, 122(3):165–170, 2025.

[5] C. Fan, M. Shen, Z. Nussinov, Z. Liu, Y. Sun, and Y.-Y. Liu. Searching for spin glass ground states through deep reinforcement learning. *Nature Communications*, 14(1):725, 2023.

[6] P. Grassberger. Percolation transitions in the survival of interdependent agents on multiplex networks, catastrophic cascades, and solid-on-solid surface growth. *Phys. Rev. E*, 91(6):062806, 2015.

[7] S.M. Hayajneh, M.I. Alzghoul, and J. Naser. Wind and slope effects on wildland fire spread: A review of experimental, empirical, mathematical, and physics-based models. *Fire*, 9(3):100, 2026.

[8] H. Hinrichsen. Non-equilibrium critical phenomena and phase transitions into absorbing states. *Advances in Physics*, 49(7):815–958, 2000.

[9] H. Hinrichsen. Non-equilibrium phase transitions. *Physica A: Statistical Mechanics and its Applications*, 369(1):1–28, 2006.

[10] B. Hof. Directed percolation and the transition to turbulence. *Nature Reviews Physics*, 5(1):62–72, 2023.

[11] C.K. Jasna and V. Sasidevan. Critical and quasicritical behavior in a three-species dynamical model of semi-directed percolation. *Journal of Statistical Mechanics: Theory and Experiment*, 2026(3):033201, 2026.

[12] D. Kapitan, P. Andriushchenko, K. Nefedev, and V. Kapitan. Convolutional neural networks application for an average thermodynamic characteristics calculation of spin glasses. In *Proc. 3rd Int. Workshop on Mathematical Modeling and Scientific Computing*, volume 104 of *EPiC Series in Computing*, pages 151–162. EasyChair, 2024.

[13] D. Kapitan, A. Korol, E. Vasiliev, P. Ovchinnikov, A. Rybin, E. Lobanova, K. Soldatov, Y. Shevchenko, and V. Kapitan. Chapter one - application of machine learning in solid state physics. In R. Macedo and R.L. Stamps, editors, *Solid State Physics*, volume 74 of *Solid State Physics*, pages 1–65. Academic Press, 2023.

[14] D. Kapitan, P. Ovchinnikov, K. Soldatov, P. Andriushchenko, and V. Kapitan. Optimized machine learning methods for studying the thermodynamic behavior of complex spin systems. *Computer Research and Modeling*, 18(1):25–40, 2026.

[15] A.O. Korol', V.Yu. Kapitan, D.Yu. Kapitan, E.V. Vasil'ev, P.A. Ovchinnikov, and K.V. Nefedev. Calculation of the ground states of spin glasses using a restricted Boltzmann machine. *JETP Letters*, 115(8):466–470, 2022.

[16] A. Maevskiy, V. Kapitan, and A. Ustyuzhanin. Artificial intelligence for multiscale modeling in solid-state physics and chemistry: A comprehensive review. *Advanced Intelligent Systems*, page 202501219, 2026.

[17] K.A. Moloney, A. Fuentes-Ramirez, and C. Holzapfel. Climate impacts on fire risk in desert shrublands: A modeling study. *Frontiers in Ecology and Evolution*, 9:601877, 2021.

[18] G. Ódor. Universality classes in nonequilibrium lattice systems. *Reviews of Modern Physics*, 76(3):663–724, 2004.

[19] P. Ovchinnikov, K. Soldatov, V. Kapitan, and G.Y. Chitov. Hierarchy of percolation patterns in a kinetic replication model. *Journal of Physics A: Mathematical and Theoretical*, 58(38):385002, 2025.

[20] P.A. Ovchinnikov, K.S. Soldatov, V.Yu. Kapitan, and G.Yu. Chitov. Hidden patterns in one-dimensional directed percolation process. *Physics of Particles and Nuclei Letters*, 22(3):540–544, 2025.

[21] D. Parkhomenko, P. Ovchinnikov, K. Soldatov, V. Kapitan, and G.Y. Chitov. Identifying internal patterns in (1+1)-dimensional directed percolation using neural networks. *Journal of Statistical Mechanics: Theory and Experiment*, 2026(10):103401, 2026. arXiv:2510.15294.

[22] A.V. Perzhu, E.V. Vasiliev, A.O. Korol, D.Yu. Kapitan, A.E. Rybin, and V.Yu. Kapitan. Application of convolutional neural networks to spin models studies. *St. Petersburg Polytechnic University Journal: Physics and Mathematics*, 58(3.1):87–92, 2022.

[23] R. Rabinovitch, Y. Biton, D. Braunstein, I. Aviram, R. Thieberger, and A. Rabinovitch. Percolation and tortuosity in heart-like cells. *Scientific Reports*, 11(1):11441, 2021.

[24] M.A. Saif and B.M. Mughalles. Determination of the critical points for systems of directed percolation class using machine learning, 2023. arXiv:2307.10456.

[25] A. Sclocchi, A. Favero, N.I. Levi, and M. Wyart. Probing the latent hierarchical structure of data via diffusion models. *Journal of Statistical Mechanics: Theory and Experiment*, 2025(8):084005, 2025.

[26] J. Shen, S. Chen, F. Liu, W. Li, and Y. Liu. Learning phase transitions by siamese neural network. *Physica A: Statistical Mechanics and its Applications*, 638:130857, 2025.

[27] J. Shen, W. Li, D. Xu, Y. Yang, Y. Wang, F. Gao, S. Wang, Y. Zhu, and K. Tuo. Machine learning of (1+1)-dimensional directed percolation based on raw and shuffled configurations. *The European Physical Journal Plus*, 139(10):944, 2024.

[28] J. Shen, F. Liu, S. Chen, D. Xu, X. Chen, S. Deng, W. Li, G. Papp, and C. Yang. Transfer learning of phase transitions in percolation and directed percolation. *Physical Review E*, 105(6):064139, 2022.

[29] K. Shiina, H. Mori, Y. Okabe, and H.K. Lee. Super-resolution of spin configurations based on flow-based generative models. *Journal of Physics A: Mathematical and Theoretical*, 57(38):385202, 2024.

[30] D. Stauffer and A. Aharony. *Introduction to Percolation Theory*. Taylor & Francis, Philadelphia, PA, USA, 2nd edition, 1992.

[31] T.F. Stepinski and J. Nowosad. The kinetic ising model encapsulates essential dynamics of land pattern change. *Royal Society Open Science*, 10(10):231005, 2023.

[32] P.N. Timonin and G.Y. Chitov. Hidden percolation transition in kinetic replication process. *Journal of Physics A: Mathematical and Theoretical*, 48(13):135003, 2015.

[33] P.N. Timonin and G.Y. Chitov. Exploring percolative landscapes: Infinite cascades of geometric phase transitions. *Physical Review E*, 93(1):012102, 2016.

[34] C. Wetterich. Probabilistic cellular automata for interacting fermionic quantum field theories. *Nuclear Physics B*, 963:115296, 2021.

[35] S. Wolfram. Statistical mechanics of cellular automata. *Reviews of modern physics*, 55(3):601, 1983.